The Canadian Mineralogist
Vol. 35, pp. 597-609 (1997)

Pt, Pd AND OTHER TRACE ELEMENTS IN SULFIDES OF THE MAIN SULFIDE ZONE, GREAT DYKE, ZIMBABWE: A RECONNAISSANCE STUDY

THOMAS OBERTHÜR[1]

Federal Institute for Geosciences and Natural Resources (BGR), Stilleweg 2, D-30655 Hannover, Germany

LOUIS J. CABRI[1]

Canada Centre for Mineral and Energy Technology (CANMET), 555 Booth Street, Ottawa, Ontario K1A 0G1

THOROLF W. WEISER[1]

Federal Institute for Geosciences and Natural Resources (BGR), Stilleweg 2, D-30655 Hannover, Germany

GREG McMAHON

Canada Centre for Mineral and Energy Technology (CANMET), 555 Booth Street, Ottawa, Ontario K1A 0G1

PETER MÜLLER

Federal Institute for Geosciences and Natural Resources (BGR), Stilleweg 2, D-30655 Hannover, Germany

Abstract

Three ore samples from the Main Sulfide Zone (MSZ) of the Great Dyke, in Zimbabwe, were investigated by a combination of mineralogical and micro-analytical techniques including optical microscopy, electron, proton, and ion microprobes. The sulfide mineralogy mainly comprises pyrrhotite + pentlandite + chalcopyrite ± pyrite. Other opaque minerals present are rutile, ilmenite, chromite, loveringite, and rare platinum-group minerals (PGM), such as sperrylite, cooperite, moncheite, and merenskyite. The micro-analytical methods employed demonstrate the presence of variable concentrations of the platinum-group elements (PGE) in pyrrhotite, pentlandite, chalcopyrite, and pyrite. The following maximum values were obtained by PIXE analysis: 64 ppmw Pt and 35 ppmw Ru in pyrrhotite, 300 ppmw Pd and 182 ppmw Rh in pentlandite, Pd, Ru and Rh below MDL in chalcopyrite, and 233 ppmw Pt and 40 ppmw Ru in pyrite. SIMS analyses confirmed the presence of Pt in pentlandite (range <0.2 to 47, mean = 8.5 ppmw), in pyrrhotite (<0.25 to 2 ppmw), in chalcopyrite (<0.15 to 3 ppmw), and consistently at elevated levels in pyrite (range 0.48–244, mean = 35.5 ppmw). These analyses are the first to report Pt concentrations in pyrite, a sulfide not previously known to be a carrier of Pt. SIMS imaging revealed a relatively homogeneous distribution of Pt in pentlandite, in contrast to its rather inhomogeneous distribution in pyrite. The integrated analytical approach has demonstrated the capability of the methods employed to unravel patterns of distribution of the PGE in the Main Sulfide Zone. Systematic investigations of profiles will be necessary to shed light on PGE metallogenesis in the Great Dyke.

Keywords: Great Dyke, platinum-group elements, trace elements, base-metal sulfides, electron microprobe, micro-PIXE, dynamic SIMS.

Sommaire

Trois échantillons de minerai provenant de la zone principale à sulfures du complexe stratiforme de Great Dyke, au Zimbabwe, ont été étudiés avec un arsenal de techniques minéralogiques et micro-analytiques, y inclus la microscopie optique et les

[1] *E-mail numbers*: thomas.oberthuer@bgr.de, louis.cabri@cc2smtp.nrcan.gc.ca, torry.weiser@bgr.de

microsondes électronique, protonique et ionique. L'assemblage de sulfures est fait de pyrrhotite + pentlandite + chalcopyrite ± pyrite. Parmi les autres minéraux opaques sont rutile, ilménite, chromite, loveringite, et, plus rarement, des minéraux du groupe du platine, tels que sperrylite, cooperite, monchéite, et merenskyite. Les méthodes micro-analytiques employées démontrent la présence de proportions variables des éléments du groupe du platine dans la pyrrhotite, la pentlandite, la chalcopyrite, et la pyrite. Les teneurs maximales suivantes ont été obtenues par analyse PIXE: 64 ppmw Pt et 35 ppmw Ru dans la pyrrhotite, 300 ppmw Pd et 182 ppmw Rh dans la pentlandite, Pd, Ru and Rh en dessous du seuil de détection dans la chalcopyrite, et 233 ppmw Pt et 40 ppmw Ru dans la pyrite. Les analyses SIMS confirment la présence de Pt dans la pentlandite (les données s'étalent entre <0.2 et 47, pour une moyenne de 8.5 ppmw), la pyrrhotite (<0.25 à 2 ppmw), la chalcopyrite (<0.15 à 3 ppmw), et indiquent systématiquement des teneurs élevées dans la pyrite (intervalle des valeurs 0.48–244, moyenne 35.5 ppmw). Ces résultats sont les premiers à indiquer des concentrations de Pt dans la pyrite, sulfure jusqu'ici insoupçonné de pouvoir l'incorporer. Les images obtenues avec la technique SIMS révèlent une distribution relativement homogène du Pt dans la pentlandite; par contre, la distribution du Pt est assez hétérogène dans la pyrite. Notre approche analytique intégrée a démontré la capacité de ces méthodes à caractériser les schémas de distribution des éléments du groupe du platine dans la zone principale à sulfures. Des études systématiques de profils choisis dans cette zone du Great Dyke seront nécessaires afin de bien comprendre la métallogenèse de ces éléments dans ce complexe igné.

(Traduit par la Rédaction)

Mots-clés: Great Dyke, éléments du groupe du platine, éléments-traces, sulfures des métaux de base, microsonde électronique, microsonde protonique, microsonde ionique.

Introduction

About 90% of the world's combined production of platinum-group elements (PGE) currently originates from South Africa and Russia. The Great Dyke of Zimbabwe constitutes the world's second largest reserve of PGE after the Bushveld Complex in neighboring South Africa (Sutphin & Page 1986). In recent years, exploration has revealed the broad pattern of mineralization, and mine production of PGE commenced in 1996 at the Hartley Platinum mine near Selous, some 70 km SW of Harare (Fig. 1). The availability of fresh underground samples, together with limited knowledge of the mineralization, prompted this study, with the aim of determining the mineralogical siting of the PGE in the ores. Two samples collected from the 160 m level reef drive of the Selous shaft and a third sample from the ore pile were used for the present pilot study. The samples were subjected to a detailed mineralogical characterization, including optical microscopy, electron-probe microanalysis (EPMA), dynamic Secondary Ion Mass Spectrometry (SIMS, also referred here as the ion microprobe), and Particle-Induced X-ray Emission (PIXE, also referred to as micro-PIXE or the proton microprobe). The proton microprobe is the ideal instrument to simultaneously determine trace amounts of most elements between Fe and Pb at the level of a few ppm (Cabri 1988). The ion microprobe, a more sensitive instrument (Chryssoulis *et al.* 1989, Chryssoulis 1990), permits analysis of sub-ppm concentrations of elements such as Au and Pt (Cabri & McMahon 1995, 1996), which have higher levels of detection with the proton microprobe, *e.g.*, 21–26 ppm Au in pyrite (Cabri *et al.* 1991) and 25–40 ppm Pt in sulfides (Cabri 1994). Previous determinations of trace levels of the PGE in Great Dyke sulfides is limited to a few electron-microprobe analyses of pentlandite for Pd by wavelength dispersion (Johan *et al.* 1989, Prendergast 1990), a technique for which minimum detection-levels for Pd are in the range of about 200 ppm (Cabri 1994).

This contribution will focus on new findings on the trace-element concentrations, especially of the platinum-group elements (PGE) in the samples studied, as determined with the ion and proton microprobes. Furthermore, the data highlight that the PGE are not only present in the form of discrete platinum-group minerals (PGM), but also are sited in various sulfides. These findings bear consequences both for metallogenetic models on PGE mineralization of the Great Dyke and for the metallurgical treatment of the ores.

Geological Setting and Sample Locations

The Great Dyke [2452 ± 14 Ma; recalculated after Hamilton (1977)] is a layered intrusion of linear shape that strikes over 550 km NNE at a maximum width of about 11 km, and cuts Archean granites and greenstone belts of the Zimbabwe craton (Worst 1960). In its present plane of erosion, the Great Dyke comprises a slightly sinuous, and locally faulted, line of five layered ultramafic–mafic complexes (the Musengezi, Darwendale, Sebakwe, Selukwe and Wedza complexes; Fig. 1). Stratigraphically, each complex is divided into a lower Ultramafic Sequence of dunites, harzburgites, olivine bronzitites and pyroxenites, together with narrow layers of chromitite, and an upper Mafic Sequence mainly consisting of a variety of plagioclase-rich rocks (norites, gabbronorites, olivine gabbros). The PGE, as well as Ni and Cu, are concentrated some meters below the transition from the Ultramafic to the Mafic Sequence, mainly in the "Main Sulfide Zone" (MSZ), several meters thick,

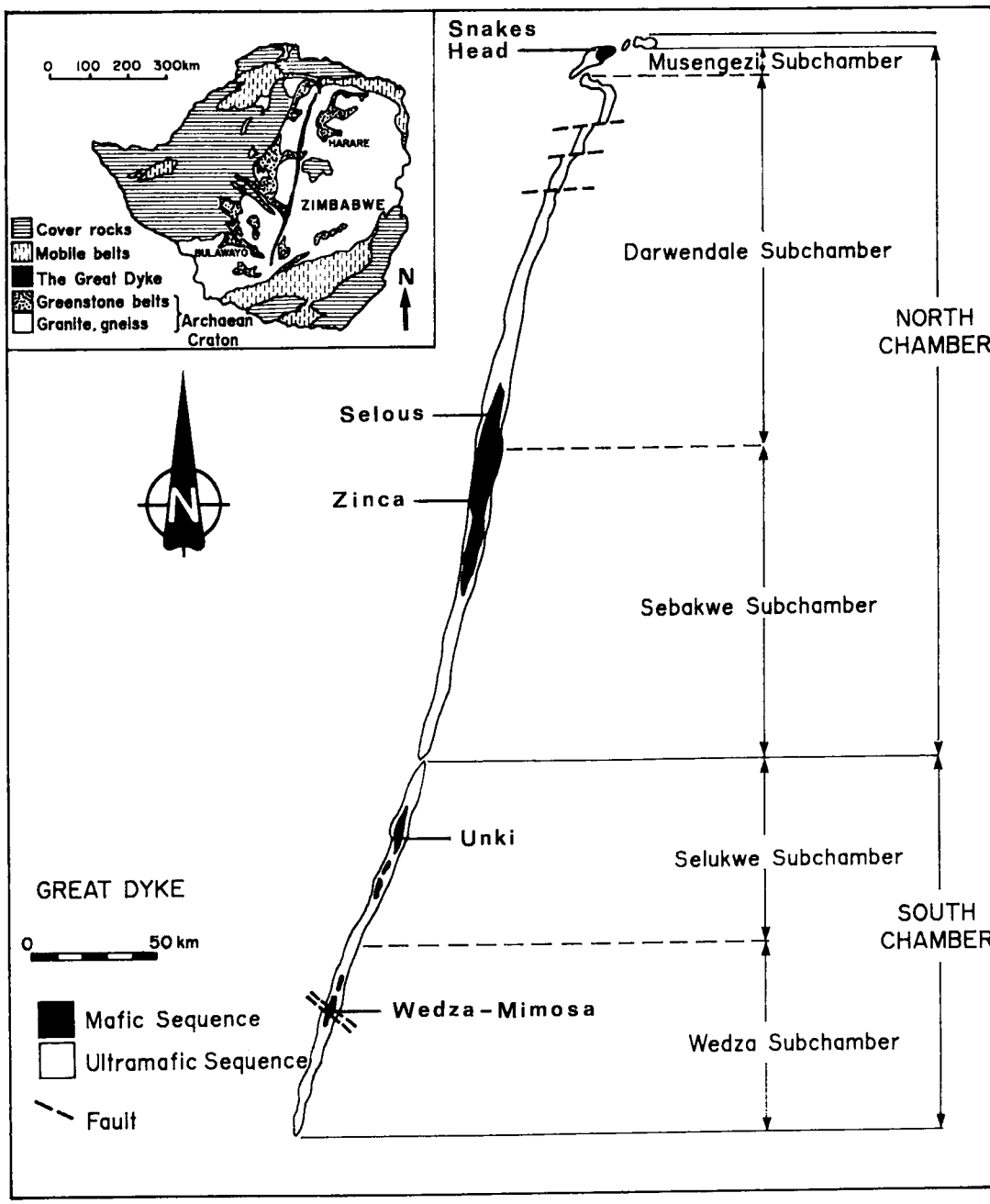

FIG. 1. Geological map of Zimbabwe showing the regional setting of the Great Dyke, and sample locality of Selous shaft, Hartley mine, Darwendale Subchamber (after Prendergast & Wilson 1989).

in pyroxenitic host-rocks. The MSZ is characterized by disseminations of sulfides (pyrrhotite, pentlandite, chalcopyrite and pyrite), which mainly occur in the form of intercumulus phases (Prendergast & Wilson 1989, Prendergast 1990, 1991, Coghill & Wilson 1993).

The samples characterized in the present study were taken in 1992 on the 160 m level reef drive of the Selous shaft, which was opened by BHP for exploration purposes. Sample ZW92/15 is from the basal part of the MSZ, whereas ZW92/14 was taken about 1 m further

up in the sequence. Sample GD–9 was collected on the ore pile close to the Selous shaft.

Sample Preparation and Analytical Methods

The samples were crushed, ground, and sieved in preparation for bulk chemical analyses. Thin and polished sections were prepared for microscopic examination, as were carbon-coated polished sections for microanalytical analyses. At BGR, thin and polished sections were investigated, and quantitative analyses of the minerals were performed using a CAMECA Camebax Microbeam electron microprobe. The analytical conditions were: accelerating voltage 20 kV, specimen current 30 nA, with 10-s measurements for the main elements and 50-s measurements for the trace elements, respectively. Natural minerals were used as standards. The raw data were corrected by using the PAP correction program supplied by CAMECA Instruments.

The proton-microprobe analyses were performed at the Scanning Proton Microprobe facility, University of Guelph, in 1994 and 1995. The analytical conditions and data reduction employed were similar to those reported by Czamanske *et al.* (1992) on sulfides from the Noril'sk–Talnakh deposits, except for the following details. In 1994, the average current used ranged from 3.75 to 6.0 nA; the charge was 2.5 μC, the beam size was approximately 10 × 20 μm, and the counting times ranged from 420 to 665 s, with the following thicknesses (in μm) of aluminum absorbers: pentlandite and chalcopyrite (352), pyrrhotite and pyrite (≅ 250). In 1995, the average current used ranged from 4.8 to 6.2 nA; the charge was 3.0 μC, the beam size was approximately 10 × 15 μm, and the counting times ranged from 480 to 630 s, with the following thicknesses (in μm) of aluminum absorbers: pentlandite (352) chalcopyrite (508), and pyrrhotite (≅ 250).

Minimum detection-levels (MDL) are largely a function of the count rates associated with the background continuum that underlies a peak of interest, and therefore vary across the spectrum. This variation, with a typical beam-charge of 3 μC using 3 MeV protons and appropriate X-ray attentuators, is given for two minerals in Figure 4 of Campbell *et al.* (1990). We define the MDL as the concentration that would result in a principal-peak intensity equal to three standard deviations of the background intensity underlying the peak. Individual MDL for specific elements are given with the results, below. Accuracies of trace-element determinations are typically 5–10%, but in favorable cases where concentrations exceed the detection limit by a factor of 100 or so, the accuracy can be as good as 1–2%.

At CANMET, the trace Pt analyses were done using a Cameca IMS–4f double-focusing magnetic sector secondary ion mass spectrometer (SIMS). Details of the operating conditions are listed in Table 1. All samples were coated with a thin film of carbon to prevent charging. In order to alleviate the problems of mass interferences associated with the ^{198}Pt mass, the mass spectrometer was operated under conditions of high mass-resolution (m/Δm ≈ 2,000), which allowed adequate separation of the mass of interest from the undesired interferences (Cabri & McMahon 1995). Local calibrations of the magnet were made, followed by depth profiles on implanted standards, as described by Cabri & McMahon (1995). To provide a reference mass for subsequent calculations of the Relative Sensitivity Factor (RSF), as well as to monitor the system's stability and the integrity of the sample, one or two other masses were recorded (*e.g.*, ^{56}Fe, $^{57}Fe_2$ + ^{32}S). The usual practice was to perform two consecutive depth-profiles on an implant standard before the mineral analyses, followed by one or two additional depth-profiles of the same implant standard at the end of the series of mineral analyses. Crater depths in the implant standard were measured using a Tencor Alpha-Step 200 profilometer several times in both directions, and RSF values were calculated using the SIMS Instrument Control System software, version 4.0, from Charles Evans and Associates. Depth profiles were then made on each mineral selected for analysis, using the same analytical procedures as for the implant standards, except that the duration of the analysis was much shorter, *e.g.*, from 200 to 400 seconds *versus* about 800 to 1,000 seconds for the implant standard. The integrated counts for ^{198}Pt and the reference mass(es) were measured from each spectrum and used, together with the average RSF value, to calculate the concentration of platinum in ppm by weight (ppmw).

Direct ion-images of selected elemental and molecular ion species were acquired by operating the instrument in the ion microscope mode while retaining high mass-resolution. In this technique, which is similar to optical

TABLE 1. SUMMARY OF THE SIMS EXPERIMENTAL PARAMETERS

Primary Ion Beam and Polarity	Cs^+
Secondary Ion Polarity	Negative
Matrix Masses Measured	^{56}Fe, $^{57}Fe_2$+^{32}S
Primary Beam Current	250-450 nA
Primary Beam Accelerating Voltage	10 kV
Impact Energy	14.5 kV
Field Aperture Diameter	750 μm
Contrast Diaphragm Diameter	400 μm
Raster	250 μm
Image Field	150 μm
Diameter of Analysis Area	62.5 μm
Implant standards: pyrite, pentlandite, chalcopyrite, pyrrhotite	
Implantation fluence, species	$1.0x10^{13}$ ions, $^{198}Pt/cm^2$
Counting time per mass per cycle	1 s
Mass resolution	~ 2,000 m/Δm
Energy offset	none
Minimum detection limits Pt: pyrite	225 - 300 ppbw
pentlandite	200 - 500 ppbw
chalcopyrite	117 - 175 ppbw
pyrrhotite	136 - 300 ppbw
Depth of analyzed profiles	0.3 - 2.0 μm

microscopy in principle, a primary ion-beam of large diameter illuminates the sample surface. Secondary ions are emitted from all points illuminated by the beam in a planar electrostatic field, such that the lateral distribution of these secondary ions is retained through the double-focusing mass spectrometer system. Following energy and mass filtering, the resulting image is recorded on a resistive anode encoder (RAE), a pulse-counting, position-computing device capable of localizing ion signals in the image plane of the detector; the ion intensity also was recorded in this image. For the present study, acquisition times ranged from 45 to 200 s, depending upon the concentration and sensitivity of the selected species.

Results

Petrography

For a detailed petrographic description of the P1 pyroxenite layer of the Great Dyke, the reader is referred to Wilson (1992). This author, Wilson *et al.* (1989), Wilson & Tredoux (1990), Prendergast (1990, 1991) and Coghill & Wilson (1993) also discussed models of the magmatic development and mechanisms of enrichment of sulfides and PGE in the P1 pyroxenite layer.

The ore-bearing bronzitites of the present study consist of subidiomorphic cumulus orthopyroxene as the main component, with plagioclase (10–15 vol.%), clinopyroxene (up to 7%) and sulfide aggregates (3–4%) occurring as interstitial phases. In addition, interstitial quartz, K-feldspar, and phlogopite are present. Quartz and K-feldspar are occasionally graphically intergrown, and phlogopite commonly contains inclusions of coarse (up to mm-size) rutile. As the sum of plagioclase + quartz + K-feldspar significantly exceeds 10 vol.%, the bronzitites should be termed melanorites according to the classification of Streckeisen (1980). The textural relationships of the interstitial silicates, and their paragenetic association with apatite, rutile, ilmenite, chromite, and loveringite, indicate that they crystallized at a late stage from a residual melt.

The post-solidification hydrous silicates present, talc and chlorite, are associated with quartz, apatite and carbonates. Notably, the interstitial aggregates of sulfides are neither intergrown with the late-stage magmatic silicates nor with the post-solidification hydrous silicates.

Ore mineralogy

The samples contain about 3–4 vol.% sulfides and traces of oxides, which mainly occur interstitially between the grains of cumulus orthopyroxene. The assemblage consists of pyrrhotite, pentlandite, chalcopyrite and subordinate pyrite; pyrite is absent in sample ZW 92/15. The sulfides either appear as small droplets within silicates or form interstitial aggregates, up to several mm across. Larger grains of sulfide are usually composed of pyrrhotite and pentlandite. Pentlandite mostly forms coarse crystalline grains; however, flame-shaped exsolution lamellae in pyrrhotite also are present. Both habits of pentlandite even coexist in larger aggregates of sulfide. Chalcopyrite tends to concentrate along the periphery of sulfide aggregates and occasionally contains some specks of mackinawite. Pyrite occurs as euhedral or subhedral grains up to 200 μm in size, commonly at the margin of or within pyrrhotite. Individual hypidiomorphic to idiomorphic crystals of pyrite locally decorate the margins of larger aggregates of sulfides, and irregular polycrystalline accumulations of pyrite are either found within or partly transect aggregates of sulfides (Fig. 2A). Notably, the latter type of pyrite is generally accompanied by chalcopyrite; locally, conspicuous symplectitic intergrowths of the two minerals are noted. Both the textures observed and the chemical data obtained on the minerals are equivocal with respect to the paragenetic position and origin of the pyrite (Fig. 2A).

Rutile is omnipresent in the ores. It forms large (mm-size) isolated rounded to oval grains or aggregates of grains usually enclosed in phlogopite. Ilmenite occurs as isolated grains (up to 200 μm in size) in the silicate matrix, or forms oriented lamellae in rutile. Rare hypidiomorphic to idiomorphic grains of chromite are up to 150 μm across. Some euhedral crystals, up to 350 μm in diameter, grey in color and weakly anisotropic, were confirmed by electron-microprobe analysis to be loveringite [(Ca,*REE*,U)(Ti,Fe,Cr,Zr,Mg,Al)$_{21}$O$_{38}$], first described from the Great Dyke by Johan *et al.* (1989).

The PGM, which include sperrylite, cooperite, moncheite, and merenskyite, are rare. They occur included in base-metal sulfides or along contacts of the sulfides with silicates (Fig. 2B). Grain sizes range from 20 to 150 μm in diameter. In addition, one 40-μm anhedral grain of gold was observed between chalcopyrite and silicate.

Electron-microprobe analyses

Pyrite, pyrrhotite and pentlandite grains from samples ZW 92/14 and GD–9 were analyzed for Fe, Ni, Co, Cu, S and Se. In sample ZW 92/15, pyrrhotite and pentlandite were analyzed. A summary of results is given in Table 2.

Eleven grains of *pyrrhotite* in sample ZW 92/14 show no major chemical variation. The Fe content is on average 60.5 wt.% (range 60.0–60.7%), that of S 39.2 wt.% (range 38.8–39.5%), and the Ni content is invariably 0.32 wt.%. Se (about 0.02 wt.%) and Cu (up to 0.03 wt.%) are also invariably present. Co could not be detected. The calculated formula is $(Fe_{0.938}Ni_{0.005})_{\Sigma 0.943D}\ S_{1.057}$. Six grains of pyrrhotite in sample ZW 92/15 have slightly lower Fe (60.3 wt.%) but higher Ni contents (0.40 wt.%), and contain about 0.02 wt.% Co, some Se (0.02 wt.%), and up to 0.07 wt.% Cu. Its formula is $(Fe_{0.988}Ni_{0.001})_{\Sigma 0.989}S_{1.109}$. Twenty grains of pyrrhotite in sample GD–9 contain, on average, 60.6 wt.% Fe, 39.2 wt.% S, and 0.3 wt.% Ni. Constant amounts of Se

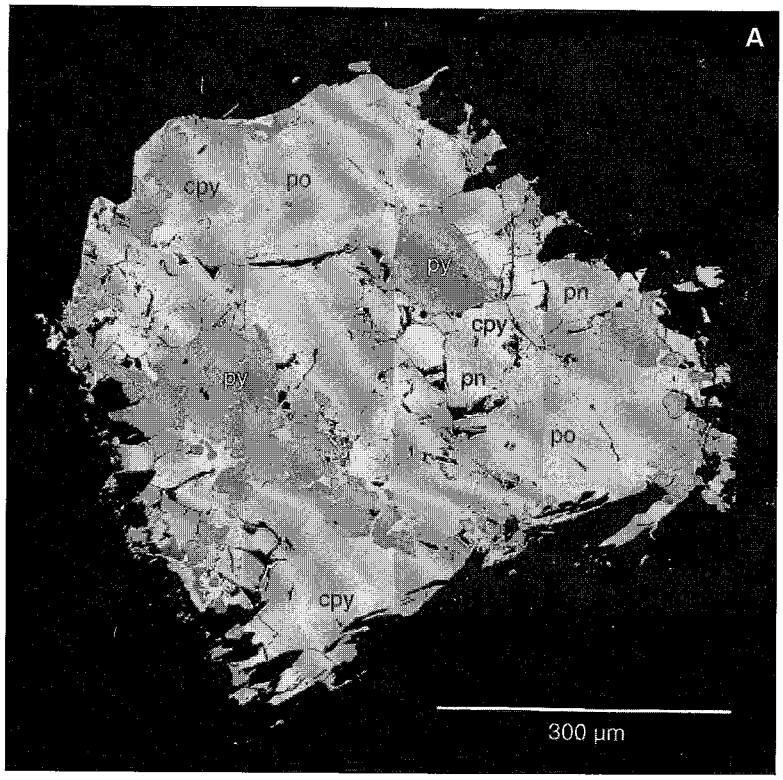

FIG. 2A. Sulfide aggregate consisting of pyrite (py, darkest grey), pyrrhotite (po, medium grey), chalcopyrite (cpy, light grey, smooth surface) and pentlandite (pn, light grey not distinguishable from chalcopyrite, but with pronounced cleavage). Sample ZW 92/14, back-scattered electron image.

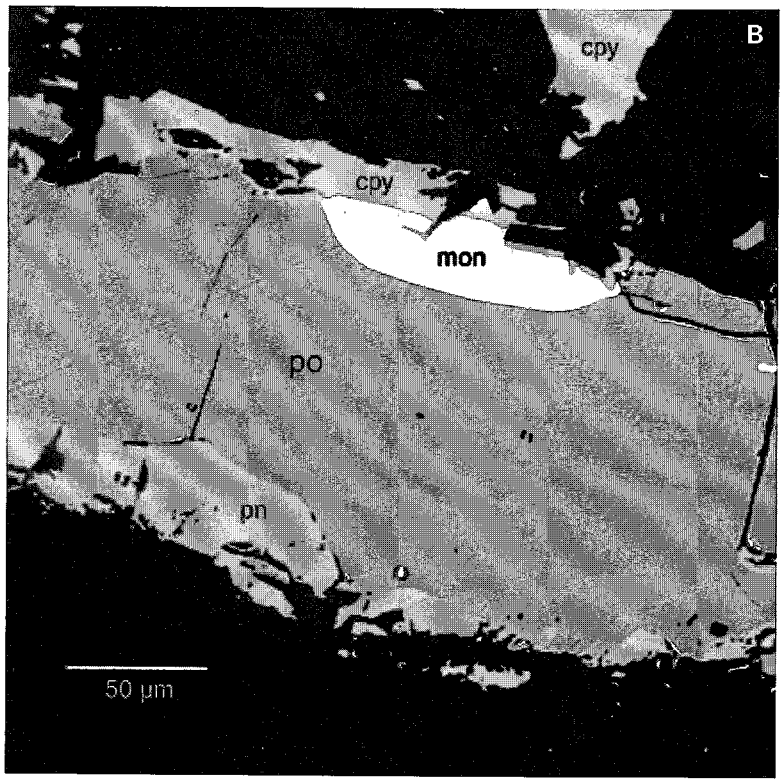

FIG. 2B. Back-scattered electron image showing moncheite (mon, white) at contact between pyrrhotite (po) and gangue (black). Chalcopyrite (cpy) and pentlandite (pn) rim pyrrhotite. Sample ZW 92/15.

TABLE 2. SUMMARY OF ELECTRON-MICROPROBE RESULTS ON PYRRHOTITE, PENTLANDITE AND PYRITE

Mineral	sample	n	Fe	Co	Ni	S	Total
Pyrrhotite	ZW 92/14	11	60.47	nd	0.32	39.16	99.95
	GD-9	20	60.57	0.01	0.30	39.20	100.08
	ZW 92/15	6	60.27	0.02	0.40	39.16	99.85
Pentlandite	ZW 92/14	15	31.46	0.53	34.87	33.08	99.94
	GD-9	37	31.37	0.44	35.22	32.87	99.90
	ZW 92/15	7	30.64	0.82	35.50	33.02	99.98
Pyrite	ZW 92/14	10	45.44	0.95	0.20	53.30	99.89
	GD-9	14	45.15	1.51	0.12	53.25	100.03

Mean values in wt.%; n: number of analyses, nd: not detected. Note that only samples ZW 92/14 and GD-9 are pyrite-bearing.

(0.02 wt.%), Cu (0.02 wt.%), and Co (0.01 wt.%) are present. The calculated formula corresponds to $(Fe_{0.938}Ni_{0.004})_{\Sigma 0.942}S_{1.057}$.

The 52 grains of *pentlandite* analyzed are chemically homogeneous, with only slight differences in the chemical composition among the three samples. The Fe content varies between 30.6 and 31.5 wt.%, the Ni content, between 35.5 and 34.9%, and the S contents range from 32.9 to 33.1%. Co shows a distinct variation, between 0.82 and 0.44 wt.%. Most of the grains contain Se (0.02 wt.%) and up to 0.25 wt.% Cu. The calculated formula of pentlandite for samples ZW 92/14 and ZW 92/15 is $(Fe_{4.290}Ni_{4.742})_{\Sigma 9.032}S_{7.971}$, and for sample GD–9, $(Fe_{4.350}Ni_{4.709})_{\Sigma 9.059}S_{7.941}$. A droplike inclusion of pentlandite in pyrite grain no. PY7 of sample ZW 92/14 has a lower concentrations of Fe (33.8 wt.%) and Ni (29.9 wt.%), and higher concentration of Co (2.4 wt.%). The calculated formula for this grain is $(Fe_{4.619}Ni_{3.883}Co_{0.310})_{\Sigma 8.802}S_{8.187}$.

Ten grains of *pyrite* in sample ZW 92/14 and 14 grains in sample GD–9, which were also analyzed by SIMS, have stoichiometric compositions. The concentrations of Ni and Cu are 0.2 wt.% and 0.1%, respectively, and Se (0.03%) is invariably present. However, Co contents vary among grains, from 0.07 to 2.2 wt.% (mean: 0.95%) in sample ZW 92/14 and from 0.11 to 2.83 wt.% (mean: 1.51%) in sample GD–9. Grain PY6, with the highest Pt content (244 ppmw) contains 0.7% Co, whereas grain PY5, with the lowest Pt content (1.3 ppmw), contains 0.87% Co. Grain PY1 contains the highest amount of Co (2.2%) and 81 ppmw Pt. This indicates that no obvious interrelationship exists between Pt and Co contents.

Proton-microprobe analyses

Selected grains of pentlandite, chalcopyrite, pyrrhotite, and pyrite from sample ZW 92/14, and of pentlandite, chalcopyrite, and pyrrhotite from sample ZW 92/15, were analyzed by micro-PIXE in two separate analytical sessions. The major results are given in Table 3.

In comparing proton-microprobe results on *pyrrhotite* in the two samples, the reader should know that over three times as many grains were analyzed from sample ZW 92/14 (33 grains) as from sample ZW 92/15 (9 grains). Pyrrhotite from sample ZW92/14 contains more Se (201 ppm average, range 156 to 243 ppm) compared to that in ZW 92/15 (average 189 ppm Se, range 162 to 221 ppm). The Se values correspond well to the EPMA average of 0.02 wt.%. Both samples contain some PGE, but because concentrations are in many cases below the MDL, the average values are not as informative. Pyrrhotite in sample ZW 92/14 contains Ru, ranging from above the MDL of 4.3 ppm to 35 ppm in 11 grains, and Rh, ranging from above the MDL of 3.6 ppm to 9 ppm in 10 grains; single grains contain Pd (6 ppm) and Pt (64 ppm), above their MDL of 5 and 38 ppm, respectively. Sample ZW 92/15 contains three grains of pyrrhotite with Rh (5 to 8 ppm) above the MDL of 4 ppm Rh, and a single grain with a concentration of 6 ppm Pd, barely above the MDL of 5 ppm Pd.

Comparison of the results on *pentlandite* between samples ZW 92/14 and ZW 92/15 shows marked differences in the concentrations of minor elements, with the single exception of Se, for which both samples have practically identical average values and ranges: 177 (110–246) ppm for sample ZW 92/14 and 175 (102–243) ppm for sample ZW 92/15. The Se contents are compatible with the EPMA of 0.02 wt.%. Pentlandite from

TABLE 3. SUMMARY OF RESULTS OF PIXE ANALYSES OF THE VARIOUS SULFIDES IN THE MSZ SAMPLES

Mineral	Sample	n	Ni	Co	Se	Cu	Pb	Zn	As	Pt	Pd	Ru	Rh	Au
Pyrrhotite	ZW 92/14	33	0.401	n.d.	201	39	44	n.d.	10	64	6	35	9	n.d.
	ZW 92/15	9	0.481	n.d.	189	31	n.d.	7	n.d.	n.d.	6	n.d.	8	n.d.
Pentlandite	ZW 92/14	36	34.52	0.826	177	769	260	n.d.	n.d.	n.a.	300	39	182	67
	ZW 92/15	30	33.06	0.934	175	n.d.	n.d.	n.d.	9	n.a.	14	7	n.a.	n.a.
Chalcopyrite	ZW 92/14	15	n.d.	n.d.	113	n.a.	133	436	6	n.a.	8	9	n.a.	42
	ZW 92/15	11	n.d.	n.d.	114	n.d.	n.d.	381	n.d.	n.a.	n.d.	n.d.	n.d.	n.a.
Pyrite	ZW 92/14	14	0.202	1.456	258	2004	96	9	6	233	9	40	10	n.a.

Concentrations of Ni and Co are expressed in wt.%, those of Se, Cu, Pb, Zn and As are in ppmw, as are those of Pt, Pd, Ru, Rh and Au. Mean values are given for Ni, Co, Se, Cu, Pb, Zn and As. Maximum values are shown for the PGE and Au. n: number of analyzed grains, n.d.: below mean limit of detection, n.a.: not analyzed. Note that only sample ZW 92/14 is pyrite-bearing.

sample ZW 92/14 is enriched in As, Ru, Rh, Pd, and Pb, and somewhat depleted in Co, Zn and Te, compared to pentlandite from sample ZW 92/15. Two values of Au (67 and 64 ppm), somewhat above the MDL (≈ 22 ppm) may be ascribed to submicrometric inclusions of gold below the surface of the section.

There are no striking differences in trace-element contents of *chalcopyrite* between samples ZW 92/14 and ZW 92/15. Se contents are remarkably similar in average values and range: 113 (96–129) ppm for sample ZW 92/14 and 114 (99–134) ppm for sample ZW 92/15. The Se concentration of chalcopyrite is the lowest among the major sulfides. Sample ZW 92/14 has slightly higher contents of Zn, Cd, and Pb; one analysis gave 8 ppm Pd (MDL = 6 ppm), and two analyses reported Au concentrations of approximately 24 ppm, slightly above the MDL, which could either be ascribed to tiny subsurface inclusions of gold or Au in the chalcopyrite structure.

The analyses of 14 grains of *pyrite* from sample ZW 92/14 indicate that it contains significant Co (1.45% average), some Ni and Cu (on average, 2,023 and 2,004 ppm, respectively), the highest concentration of Se of all sulfides analyzed (258 ppm, range 197 to 316 ppm), as well as PGE. The average Ni and Se concentrations in pyrite analyzed by EPMA and by micro-PIXE are virtually identical. Both analytical methods measured the level of Co as well (0.95 wt.% *versus* 1.45 wt.%), but average results of PIXE analyses are somewhat higher. This difference may be due to the different number of grains averaged or inhomogeneity in the Co distribution, which is reflected in different volumes analyzed (*e.g.*, 12 μm³ for EPMA and 1,700 μm³ for PIXE). The high average Cu content is probably due to subsurface inclusions of chalcopyrite in four grains. Eight of 14 grains contain Ru above a MDL of 3.8 ppm; they average 8 ppm and attain 40 ppm Ru, the highest value recorded for all the sulfides analyzed. Four out of 14 grains contain Rh and Pd concentrations above their MDL of 4 and 3.4, respectively. In addition, three grains have Pt concentrations above the MDL of 44 ppm and range from 47 to 233 ppm Pt.

TABLE 4. CONCENTRATIONS OF Pt IN BASE-METAL SULFIDES AS ESTABLISHED BY SIMS

Mineral	n	MDL	mean	range
pyrrhotite	23	0.30	—	<MDL - 2
pentlandite	28	0.50	8.5	<MDL - 47
chalcopyrite	12	0.18	1.3	<MDL - 3
pyrite	37	0.30	35.5	0.4 - 244

n: number of measured grains. Concentrations are expressed in ppmw.

Ion-microprobe analyses and ion imaging

On the basis of the results of the PIXE studies, selected grains of pentlandite, chalcopyrite, pyrrhotite,

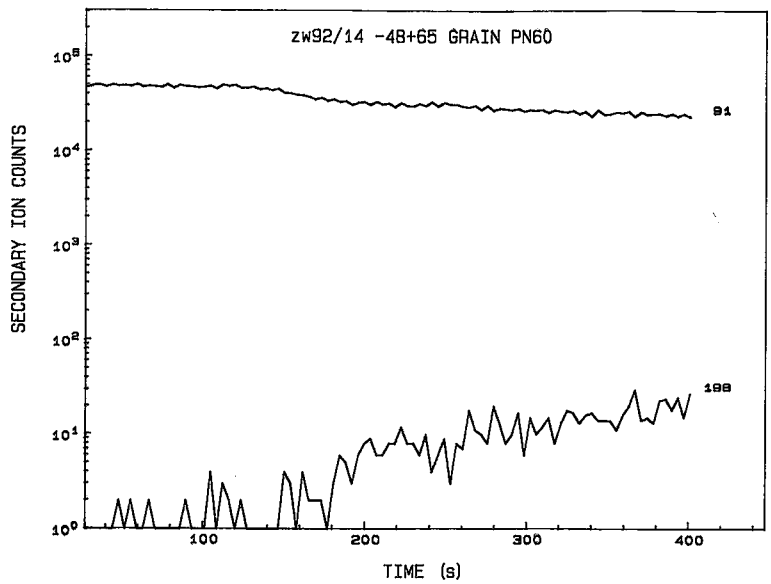

FIG. 3. SIMS depth profile of grain PN60, showing a zone with little Pt (up to about 180 s), averaging about 0.42 ppmw Pt, and a zone with increasing Pt concentration (averaging 3.3 ppmw Pt). The slight drop in matrix counts (mass 91) coincides with the increase in Pt concentration and may reflect a compositional change in major and minor elements.

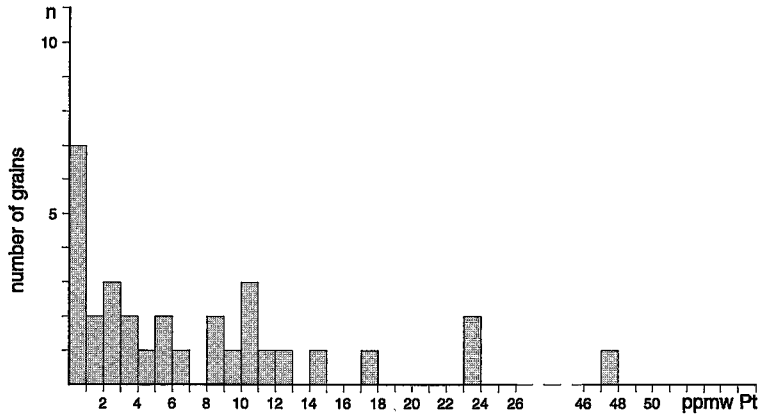

FIG. 4. Histogram of Pt concentrations (in ppmw) in pentlandite.

and pyrite were analyzed for Pt by dynamic SIMS. A summary of the results is given in Table 4.

A total of 23 grains of *pyrrhotite* were analyzed. A characteristic of the depth profiles is zoning of Pt concentration, as seen in seven grains. Depth profiles of some grains showed as many as four different zones, with distinct concentrations. About half the grains analyzed have Pt concentrations less than the MDL; the rest range up to a maximum value of 2 ppm Pt.

The range of Pt concentration measured in 28 grains of *pentlandite* is from less than the MDL to a single high value of 47.4 ppm Pt in grain PN21, which also has a zone with relatively little Pt (0.76 ppm). Re-analysis of this grain (*i.e.*, analysis of a deeper part of the grain) gave a concentration of 9.2 ppm Pt. A second zoned grain of pentlandite (PN60) displays a smaller difference in concentration between the two zones (0.42 and 3.3 ppm), as shown in Figure 3. Most of the pentlandite grains analyzed have Pt concentrations between 1 and 18 ppm (Fig. 4).

Of 12 grains of *chalcopyrite* analyzed for Pt, three show evidence of some zoning with depth; most have Pt concentrations from less than the MDL to about 1 ppm Pt. Two grains have exceptionally higher Pt concentrations, reaching over 3 ppm in certain zones.

All 37 grains of *pyrite* analyzed contain Pt in concentrations above the minimum detection-level of 225 to 300 ppbw. The range of concentrations measured was from 1.29 to 244 ppmw Pt for pyrite in sample ZW 92/14/(–65+100) and ZW/92/14/Section 1, from 0.42 to 58.2 ppmw Pt for pyrite in sample ZW 92/14/ Section 2, and from 0.48 to 118 ppmw Pt for pyrite in sample GD–9. In a plot of all analytical results on pyrite as one population on a frequency diagram (Fig. 5), the majority lie between 1 and 50 ppm, with most being between 1 and 25 ppm. Results of individual analyses are listed in Table 5.

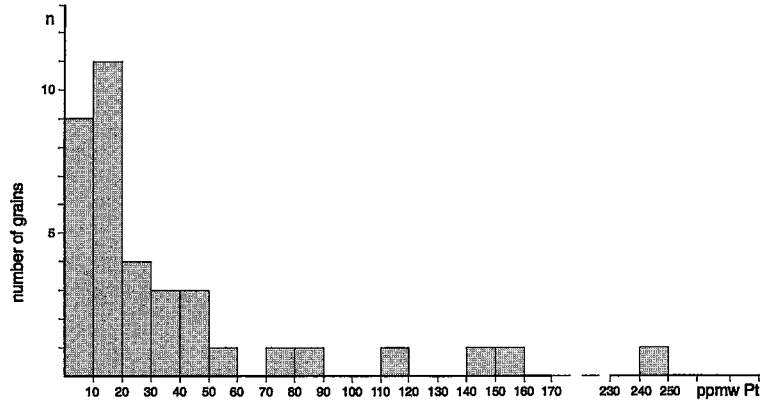

FIG. 5. Histogram of Pt concentrations (in ppmw) in pyrite.

TABLE 5. CONCENTRATIONS OF Pt IN PYRITE: RESULTS OF ION-MICROPROBE ANALYSES

Sample	Grain No.	Pt (ppmw)	Comments
ZW/92/14 (-65+100)	PY1	81.145	imaged
ZW/92/14 (-65+100)	PY2	46.209	
ZW/92/14 (-65+100)	PY3	140.486	octahedral cross-section; imaged
ZW/92/14 (-65+100)	PY4	35.928	imaged
ZW/92/14 (-65+100)	PY5	1.288	
ZW/92/14 (-65+100)	PY6	244.433	
ZW/92/14 (-65+100)	PY7	23.765	octahedral cross-section
ZW/92/14 (-65+100)	PY8	158.227	
ZW/92/14 (-65+100)	PY9	74.647	imaged
ZW/92/14 (-65+100)	PY10	19.519	
ZW/92/14 (-65+100)	PY11	10.149	
ZW92/14 Section 1	94-012	24.870	
ZW92/14 Section 1	94-036R	35.613	
ZW92/14 Section 1	94-042	6.644	
ZW92/14 Section 1	94-068	17.981	
ZW92/14 Section 1	94-050	1.405	
ZW92/14 Section 1	94-056	9.783	
ZW92/14 Section 1	94-056R	17.178	
ZW/92/14 Section 2	PY12	0.418	
ZW/92/14 Section 2	PY13	3.741	
ZW/92/14 Section 2	PY14	18.683	
ZW/92/14 Section 2	PY15	58.241	
ZW/92/14 Section 2	PY16	4.205	
GD-9	PY1	24.456	
GD-9	PY2	31.587	
GD-9	PY3	47.219	imaged
GD-9	PY4	18.231	
GD-9	PY5	48.510	
GD-9	PY5a	118.269	imaged
GD-9	PY6	16.103	
GD-9	PY7	0.483	
GD-9	PY8	12.451	
GD-9	PY9	4.541	
GD-9	PY11	15.935	
GD-9	PY12	18.302	
GD-9	PY13	14.101	
GD-9	PY14	26.311	

Imaging of the distribution of Pt was performed on pyrite and pentlandite. In the case of pyrite, six grains were imaged, and the Pt was found to be distributed relatively inhomogeneously. The direct-ion images of the Pt concentration resemble those illustrating the distribution of Au in pyrite and arsenopyrite (*e.g.*, Cabri *et al.* 1991, Cabri & McMahon 1996, Chryssoulis 1990, Fleet *et al.* 1993, Oberthür *et al.* 1994); though inhomogeneous, there is no evidence of submicrometric inclusions in the depth profiles or of discrete "hot spots" in the ion images. Where pyrite is intergrown with pentlandite, the Pt occurs only in pyrite (Fig. 6). The preference of Pt for pyrite over pyrrhotite can also be seen in Figure 7, which also includes images for three Pt masses: ^{194}Pt, ^{195}Pt and ^{198}Pt. Though these were done sequentially, and therefore represent different sputtered volumes, the sum of the Pt counts for each of the three masses corresponds to their expected natural isotopic abundances, further confirmation that these are indeed images of Pt in pyrite. A total of five grains of pentlandite were imaged for several Pt isotopes (^{194}Pt, ^{195}Pt and ^{196}Pt) to confirm, through the sums of the Pt counts, that their ratios correspond to theoretical values. Because the Pt concentration in pentlandite is less than that found in pyrite, the images of Pt are not as intense, and suggest a more uniform distribution of Pt. An occasional localized increase in Pt concentration, however, gives an indication of inhomogeneity. No correlations could be discerned with other elements (*e.g.*, Ni, Fe, Cu).

Summary

The present reconnaissance study has provided a first insight into the distribution of PGE in the Main Sulfide Zone of the Great Dyke, though the limited data are not yet sufficient to formulate rules concerning the distribution of the PGE. The study, however, has shown the following:

(i) Pyrrhotite, pentlandite and chalcopyrite, the principal sulfides, form a simple paragenesis, whereas pyrite is present only locally. Two sample groups, tentatively divided into pyrite-free and pyrite-bearing, show marked differences in the trace-element contents of their sulfides: pyrite-bearing samples have pyrrhotite with lower Ni contents (mean 0.30 *versus* 0.40 wt.%) and pentlandite with lower Co contents (0.44 *versus* 0.82 wt.%). At the same time, the pyrite-bearing samples have distinctly higher concentrations of the PGE in pyrrhotite and pentlandite compared to the pyrite-free sample. The pyrite is Co- and Ni-bearing (up to 2.83 and 0.39 wt.%, respectively), and was identified as a major, consistent host of Pt. The latter finding is of particular importance, as pyrite previously has not been known to be a carrier of Pt (Cabri 1994).

(ii) Oxide minerals include rutile, ilmenite, chromite and loveringite. The unusual compositions of the oxide minerals reported by Johan *et al.* (1989) are substantiated by electron-microprobe analyses performed in this study. The rutile is Cr- and Zr-bearing (wt.% level in each case), chromite has up to 2.82 wt.% TiO_2, together with low Mg contents (0.67–3.23 wt.% MgO), and loveringite is a collector of a wide spectrum of incompatible elements. These mineral compositions are attributed to crystallization from a residual melt, possibly with participation of a late-magmatic fluid phase.

(iii) The PGE investigated (*i.e.*, Pt, Pd, Rh, Ru) are bimodally distributed in the ores, being present in the form of discrete PGM, and also occurring in appreciable though variable amounts in sulfides, probably in solid solution. It is notable that only sulfides of the pyrite-bearing samples of our study carry the PGE at meaningful average concentrations, which also indicate partitioning of the PGE into various sulfides. Most of the Pd and Rh is concentrated in pentlandite (mean contents: 207 and 29 ppmw, respectively), and Pt is mainly found in pyrite (mean: 35.5 ppmw). Whether

the observed differences among the samples reflect the "normal" spectrum of the MSZ mineralization or represent systematic trends of cryptic variation in the MSZ is still an open question. The absence of magnetite in all samples and the occasional presence of pyrite indicate variable and relatively elevated conditions of $f(S_2)$ and $f(O_2)$.

A more detailed study of the PGE distribution in sulfides, including mineralogical–geochemical balances, and information on PGM parageneses in the MSZ, are needed to unravel the rules and timing of PGE mobilization and PGM crystallization. Our approach of using a wide range of microbeam techniques has demonstrated the capability of the methods employed to further our

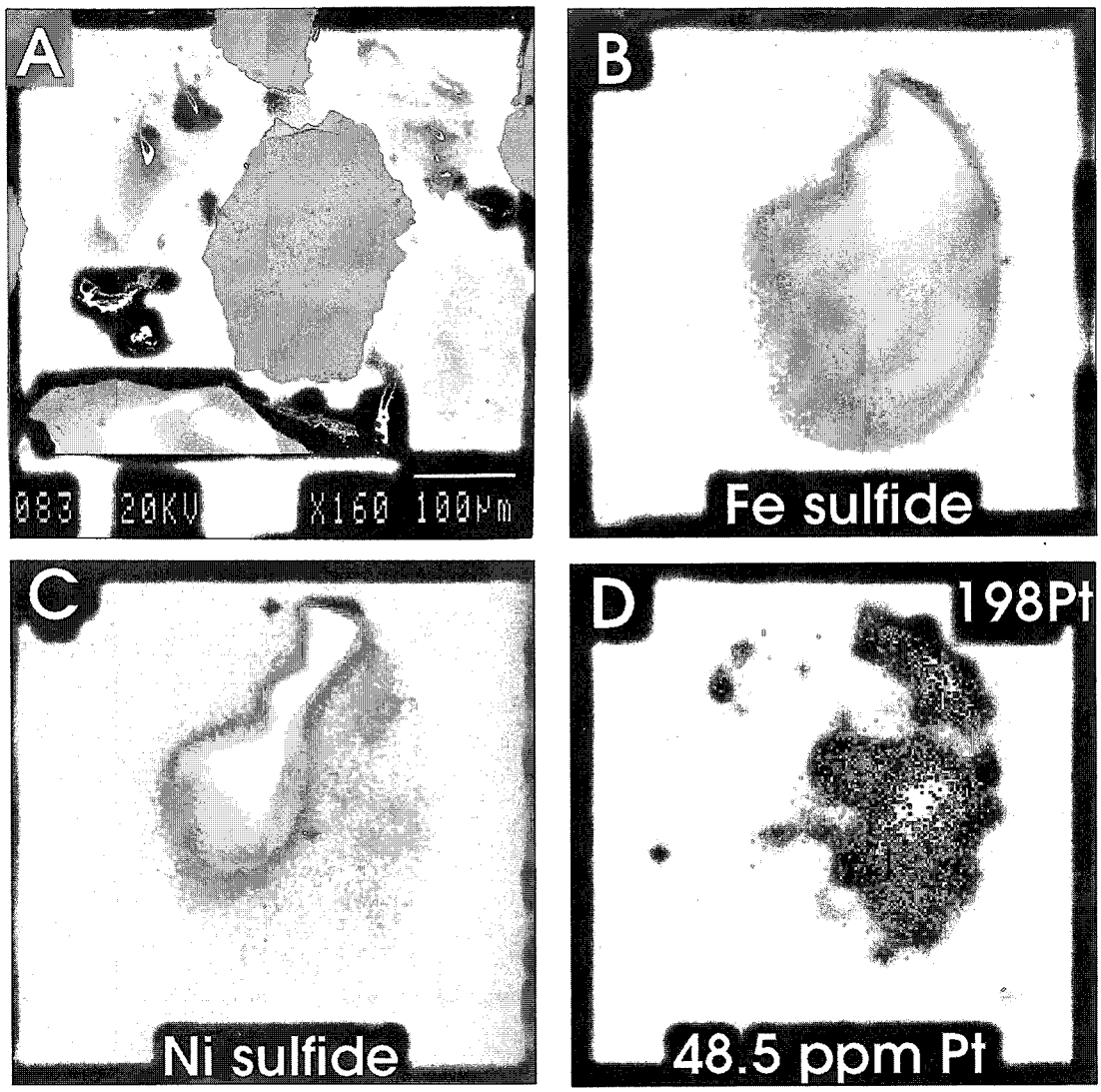

FIG. 6. A. Back-scattered electron image of a pyrite grain with attached pentlandite visible on top of grain PY1 (sample ZW/92/14/–65+100), taken after the ion microprobe images. B. Direct-ion image of an iron sulfide mass of same composite grain, in which the outline of the grain edge may be compared to the BSE image (slightly rotated). C. Direct-ion image of a nickel sulfide mass corresponding to the pentlandite in the BSE image. D. Direct-ion image of ^{198}Pt, indicating its preference for pyrite (48.5 ppmw Pt) rather than pentlandite. Diameter of field for the ion images is 62.5 µm in each case; the images were taken sequentially, beginning with B.

knowledge on the patterns of PGE distributions in the MSZ ores. We intend to systematically investigate complete MSZ profiles using combined mineralogical and micro-analytical techniques in order to increase the level of understanding of PGE metallogenesis in the Great Dyke.

ACKNOWLEDGEMENTS

Our sincere thanks go to G.L. Holland, Manager Resource Planning, BHP World Minerals, Harare, for allowing access to and sampling at the Hartley Platinum operations, and assistance in the field and later with data interpretation. Over many years, the Geological Survey of Zimbabwe, the Geology Department and the Institute of Mining Research of the University of Zimbabwe, all at Harare, were helpful partners in all aspects of our work in Zimbabwe. Technical support is acknowledged in the form of sample preparation and some SEM work at CANMET by M.J. Beaulne, D. Carson, and J.H.G. Laflamme. The electron microprobe analyses were performed by J. Lodziak at BGR. Thoughtful reviews by the Editor and two anonymous referees are acknowledged with thanks.

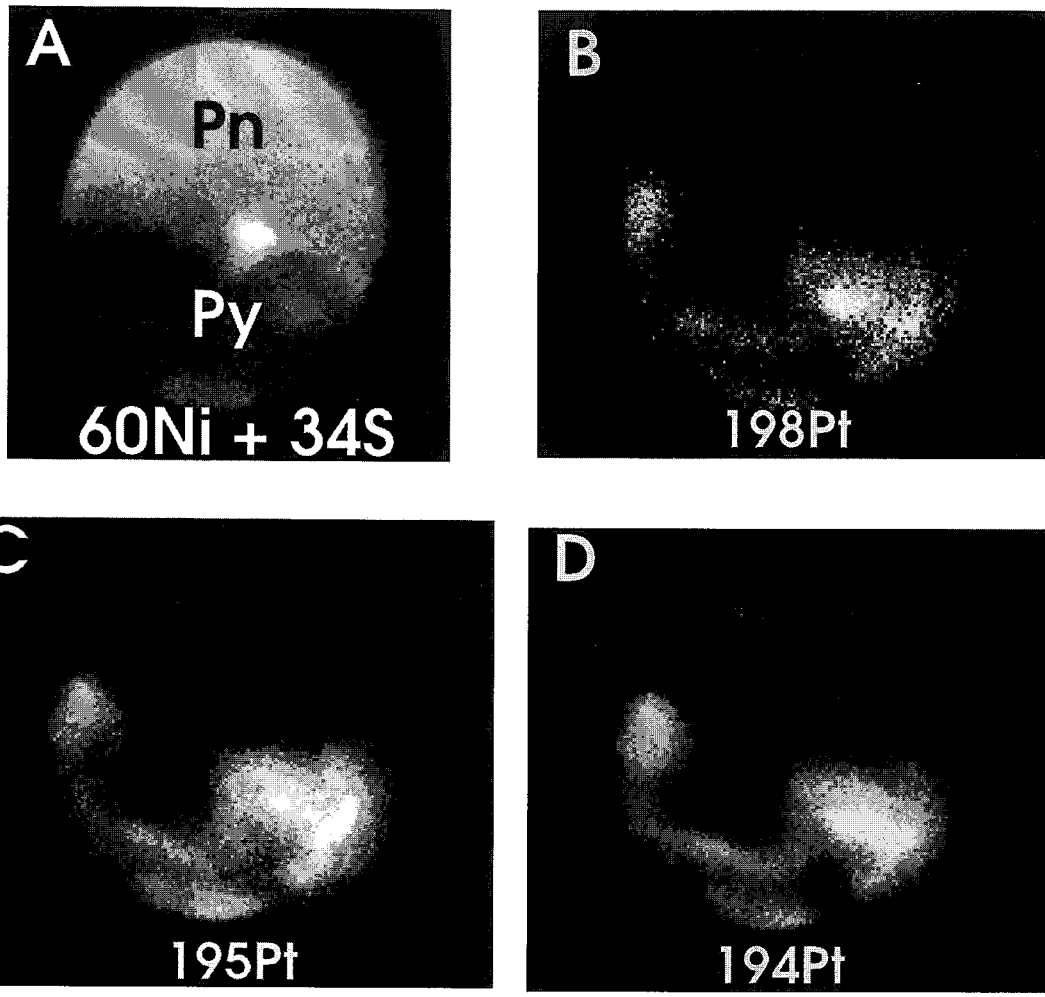

FIG. 7. A. Direct-ion image of an iron sulfide mass of an area of composite grain consisting of pentlandite (top) and pyrite (bottom, grain PY5a, sample GD–9). Direct-ion image of the nickel sulfide distribution, restricted to the pentlandite. B. Direct-ion image showing the distribution of ^{198}Pt, restricted to the pyrite. C. Direct-ion image showing the distribution of ^{195}Pt in the pyrite. D. Direct-ion image showing the distribution of ^{194}Pt in the pyrite. Total concentration of Pt in pyrite is 118 ppmw. Diameter of field for the ion images is 62.5 μm in each case; the images were taken sequentially beginning with A.

REFERENCES

CABRI, L.J. (1988): Applications of proton and nuclear microprobes in ore deposit mineralogy and metallurgy. *Nucl. Instrum. Methods Phys. Res.* **B30**, 459-465.

_____ (1994): Current status of determination of mineralogical balances for platinum-group element-bearing ores. *Trans. Inst. Mining Metall., Sect. B: Appl. Earth Sci.* **103**, B3-9.

_____, CHRYSSOULIS, S.L., CAMPBELL, J.L. & TEESDALE, W.J. (1991): Comparison of in-situ gold analyses in arsenian pyrite. *J. Appl. Geochem.* **6**, 225-230.

_____ & MCMAHON, G. (1995): SIMS analysis of sulfide minerals for Pt and Au: methodology and Relative Sensitivity Factors (RSF). *Can. Mineral.* **33**, 349-359.

_____ & _____ (1996): The quantitative determination of sub-ppm quantities of Au and Pt in sulfide minerals. *In* Proc. Extraction and Processing Division Congress (G.W. Warren, ed.). The Minerals, Metals & Materials Society, Warrendale, Pennsylvania (313-322).

CAMPBELL, J.L., MAXWELL, J.A., TEESDALE, W.J., WANG, J.-X. & CABRI, L.J. (1990): Micro-PIXE as a complement to electron probe microanalysis in mineralogy. *Nucl. Instrum. Methods Phys. Res.* **B44**, 347-356.

CHRYSSOULIS, S.L. (1990): Quantitative trace metal analysis of sulfide and sulfarsenide minerals by SIMS. *In* Proc. Secondary Ion Mass Spectroscopy, SIMS VII (A. Benninghoven, C.A. Evans, K.D. McKeegan, H.A. Storms & H.W. Werner, eds.). John Wiley & Sons, Chichester, U.K. (405-408).

_____, CABRI, L.J. & LENNARD, W. (1989): Calibration of the ion microprobe for quantitative trace precious metal analyses of ore minerals. *Econ. Geol.* **84**, 1684-1689.

COGHILL, B.M. & WILSON, A.H. (1993): Platinum-group minerals in the Selukwe subchamber, Great Dyke, Zimbabwe: implications for PGE collection mechanisms and post-formational redistribution. *Mineral. Mag.* **57**, 613-633.

CZAMANSKE, G.K., KUNILOV, V.E., ZIENTEK, M.L., CABRI, L.J., LIKHACHEV, A.P., CALK, L.C. & OSCARSON, R.I. (1992): A proton-microprobe study of magmatic sulfide ores from the Noril'sk–Talnakh district, Siberia. *Can. Mineral.* **30**, 249-287.

FLEET, M.E., CHRYSSOULIS, S.L., MACLEAN, P.J., DAVIDSON, R. & WEISENER, C.G. (1993): Arsenian pyrite from gold deposits: Au and As distribution investigated by SIMS and EMP, and color staining and surface oxidation by XPS and LIMS. *Can. Mineral.* **31**, 1-17.

HAMILTON, J. (1977): Sr isotope and trace element studies of the Great Dyke and Bushveld mafic phase and their relation to early Proterozoic magma genesis in southern Africa. *J. Petrol.* **18**, 24-52.

JOHAN, Z., OHNENSTETTER, D. & NALDRETT, A.J. (1989): Platinum-group minerals and associated oxides and base metal sulphides of the Main Sulphide Zone, Great Dyke, Zimbabwe. *In* Fifth Int. Platinum Symp., Abstr. (H. Papunen, ed.). *Bull. Geol. Soc. Finland* **61**(1), 53-54.

OBERTHÜR, T., VETTER, U., SCHMIDT MUMM, A., WEISER, T., AMANOR, J.A., GYAPONG, W.A., KUMI, R. & BLENKINSOP, T.G. (1994): The Ashanti gold mine at Obuasi, Ghana: mineralogical, geochemical, stable isotope and fluid inclusion studies on the metallogenesis of the deposit. *Geol. Jahrb.* **D 100**, 31-129.

PRENDERGAST, M.D. (1990): Platinum-group minerals and hydrosilicate "alteration" in Wedza–Mimosa platinum deposit, Great Dyke, Zimbabwe – genetic and metallurgical implications. *Trans. Inst. Mining Metall., Sect. B: Appl. Earth Sci.* **99**, B91-105.

_____ (1991): The Wedza–Mimosa platinum deposit, Great Dyke, Zimbabwe: layering and stratiform PGE mineralisation in a narrow mafic magma chamber. *Geol. Mag.* **128**, 235-249.

_____ & WILSON, A.H. (1989): The Great Dyke of Zimbabwe. II. Mineralisation and mineral deposits. *In* Magmatic Sulphides – the Zimbabwe Volume (M.D. Prendergast & M.J. Jones, eds.). The Institution of Mining and Metallurgy, London, U.K. (21-42).

STRECKEISEN, A. (1980): Classification and nomenclature of volcanic rocks, lamprophyres, carbonatites and melilitic rocks. IUGS subcommission on the systematics of igneous rocks, recommendations and suggestions. *Geol. Rundschau* **90**, 194-207.

SUTPHIN, D.M. & PAGE, N.J. (1986): International strategic minerals inventory summary report – platinum-group metals. *U.S. Geol. Surv., Circ.* **930-E**.

WILSON, A.H. (1992): The geology of the Great Dyke, Zimbabwe: crystallization, layering and cumulate formation in the P 1 Pyroxenite of Cyclic Unit 1 of the Darwendale Subchamber. *J. Petrol.* **33**, 611-663.

_____, NALDRETT, A.J. & TREDOUX, M. (1989): Distribution and controls of platinum-group element and base metal mineralisation in the Darwendale Subchamber of the Great Dyke, Zimbabwe. *Geology* **17**, 649-652.

_____ & TREDOUX, M. (1990): Lateral and vertical distribution of the platinum group elements, and petrogenetic controls on the sulfide mineralization in the P 1 Pyroxenite layer of the Darwendale Subchamber of the Great Dyke, Zimbabwe. *Econ. Geol.* **85**, 556-584.

WORST, B.G. (1960): The Great Dyke of Southern Rhodesia. *S. Rhod. Geol. Surv., Bull.* **47**.

Received July 15, 1996, revised manuscript accepted December 28, 1996.